Surface and bulk photoresponse of crystalline As_2S_3

D. F. Blossey and R. Zallen
Xerox Webster Research Center, Webster, New York 14580
(Received 20 December 1973)

The steady-state photoresponse of the layer-structure crystal As_2S_3 is reported as a function of wavelength, light intensity, and electric field strength, using aqueous salt solutions as transparent electrodes. The photocurrent spectrum follows the edge-absorption spectrum for photon energies near and above the optical bandgap (2.7 eV), but not for longer wavelengths. In the long-wavelength photoresponse, a unique interference effect is observed which identifies the underlying mechanism as photoinjection of electrons from surface states. For bulk absorbed light, the photocarrier generation efficiency is in the range of 0.1 to 1.0, is ambipolar, is independent of light intensity, and shows a field dependence consistent with the Onsager model. From Onsager theory a thermalization length for hot carriers is calculated to be 40 Å. The dark resistivity perpendicular to the layers is measured to be 3×10^{15} Ω cm.

I. INTRODUCTION

There are two principal reasons for studying the crystalline arsenic chalcogenides, As_2S_3 and As_2Se_3. The first is that their layered structure provides a unique opportunity for studying both weak and strong bonding effects in the same crystal. The second is to provide reference points for studies on amorphous As_2S_3 and As_2Se_3 so that distinction between effects due to chemical composition and those due to structural form can be made.

Because the layered crystals As_2S_3 and As_2Se_3 are held together by both weak and strong bonds, they are, in the most general sense, *molecular crystals in which the molecular unit is macroscopically extended in two dimensions*. As in any molecular system, the extent of a molecular unit is defined by the extent of the strong-bonding network. In the layer-structure chalcogenides, the strong bonding within the layer is primarily covalent. The bonding between layers is much weaker and, as is the case in most molecular solids, is less well defined than the intralayer bonding. As a result of their layered structures, these crystals behave, in many ways, as covalent (two-dimensional-network) crystals in two spatial directions but as molecular crystals in the third and thereby provide unique opportunities for sorting out intramolecular and intermolecular effects.[1]

The second motivating force for the study of these crystals is the interest in their relationship to the corresponding amorphous solids, a-As_2S_3 and a-As_2Se_3. While recent intensive efforts on three-dimensional-network amorphous solids such as a-Ge and a-Si have proceeded in the presence of, and certainly with assistance from, the wealth of knowledge that has been generated about the corresponding crystals, quite the opposite is true for the chalcogenides. In fact, very little is known about crystalline As_2S_3 and As_2Se_3 while their amorphous forms have been heavily studied due to their technological importance as infrared-transmitting glasses and visible-light photoconductors. Since many measurements have been performed on the amorphous chalcogenides without prior knowledge of the crystalline properties, it has not always been clear which properties were characteristic of the chemical composition and which were characteristic of the structural form. A good example of a point of confusion is in transport studies on amorphous chalcogenides in which a frequency-dependent ac conductivity is interpreted in terms of hopping within disorder-induced band-tail states.[2] However recent measurements have now shown that crystalline As_2S_3 (as well as other molecular crystals) also exhibits a frequency-dependent ac conductivity,[3] so that the hopping states cannot be a result of disorder.

In this paper we report studies of the photoconductivity of crystalline As_2S_3 in which we observe both electron photoinjection from surface states and field-dependent bulk generation of photocarriers. The surface states occur at energies within the crystal's forbidden gap and may be present as defect states in the bulk of the amorphous form. Field-dependent photogeneration is observed in amorphous Se,[4] As_2S_3,[5] and other amorphous molecular solids[6] but is also present in other molecular crystals such as anthracene.[7] This effect is clearly not a result of disorder but appears to be a more general property of low-mobility solids, as the frequency-dependent ac conductivity may well be. Photoconductivity is a three-step process involving optical absorption, charge separation of electron-hole pairs (carrier generation), and transport of the carriers through their respective bands. Thus it is important to examine each of these processes in detail and any dependencies on structural form.

The structure[8] of crystalline As_2S_3 (orpiment) is shown in Fig. 1. Orpiment is a relatively complex low-symmetry layer-structure crystal. The crystal symmetry[8] is monoclinic (C_{2h}^5), while the diperiodic symmetry of an individual layer is orthorhombic (C_{2v}^7). Crystals are pale yellow in color and show pronounced micaceous (010) cleavage parallel to the layers. The optical properties for light polarized in the layer plane ($\vec{E} \parallel \vec{a}$, $\vec{E} \parallel \vec{c}$) have been reported[9,10] and it has been demonstrated that it is the layer symmetry (rather than the crystal symmetry) which dominates both the electronic[10] and lattice[1] spectra. Thus the optical properties of the solid are largely those of the isolated molecule (the extended layer) and reflect primarily strong-bonding intralayer effects.

While optical absorption is mainly intramolecular in nature, electronic transport is a very different story. Conductivity perpendicular to the layers is necessarily controlled by the weak interlayer interactions. Drift-mobility measurements[11] have placed the carrier mobilities for transport perpendicular to the layers in the vicinity of 1 cm^2/V sec for both electrons and holes. These mobility values are quite typical of molecular solids such as organic crystals,[12,13] in which carrier transport occurs across weak bonds.

The experimental setup and some preliminary results are discussed in Sec. II, the interference effects and surface photoresponse in Sec. III, the field-dependent bulk generation in Sec. IV, and a summary is contained in Sec. V.

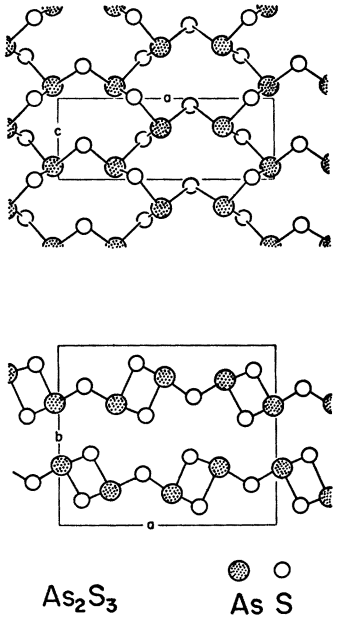

FIG. 1. Orpiment structure.

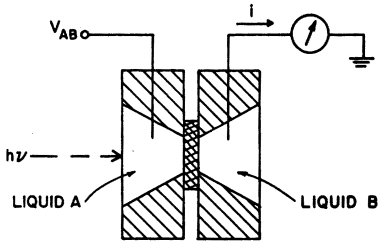

LIQUID ELECTRODE CELL

FIG. 2. Schematic of liquid electrode cell.

II. EXPERIMENTAL AND PRELIMINARY RESULTS

The crystals used in these experiments were cleaved from natural orpiment crystals.[1,10] The experiment was carried out in a sandwich-cell configuration shown schematically in Fig. 2. The contacts that were used were transparent aqueous 1-M NaI solutions; results were insensitive to type of salt used in the electrolytes (NaI, NaCl, KI, etc.). Exciting radiation was provided by a Ge-DXN 1000-W tungsten lamp, with the light filtered through a Leiss-prism double monochromator. The spectral slit width employed was less than 20 meV, with typically 10^{11} photons sec^{-1} hitting the active sample area of 0.044 cm^2. The photon flux was measured using a calibrated EG&G-type SGD-100A photodiode. The windows in the liquid electrode cell were quartz, and platinum wires were used to make electrical contact to the liquids. The voltage was provided by a Fluke 412B power supply and the current through the sample was monitored

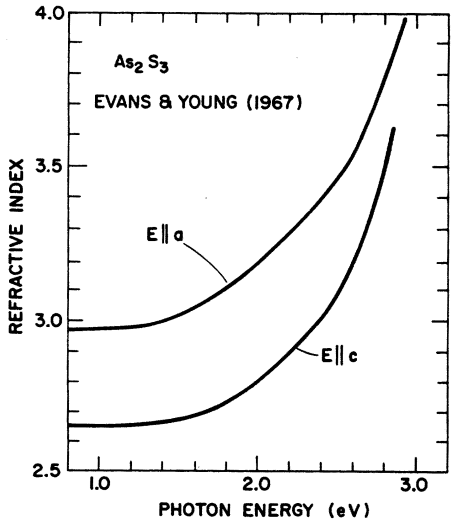

FIG. 3. Refractive indices for crystalline As_2S_3 for light polarized in the layer plane ($\vec{E} \parallel \vec{a}$, $\vec{E} \parallel \vec{c}$).

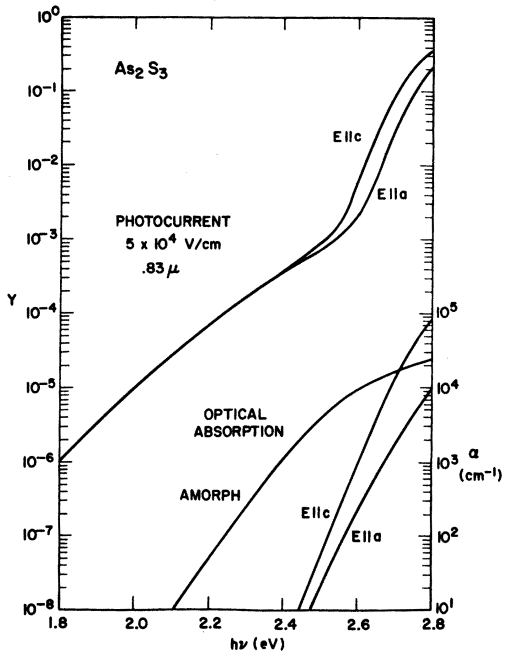

FIG. 4. Photoyield (Y) spectrum and edge-absorption spectrum of crystalline As_2S_3 for light polarized $\vec{E} \parallel \vec{c}$ and $\vec{E} \parallel \vec{a}$. Edge-absorption spectrum for amorphous As_2S_3. The photoyield is the photocurrent density normalized to incident photon flux.

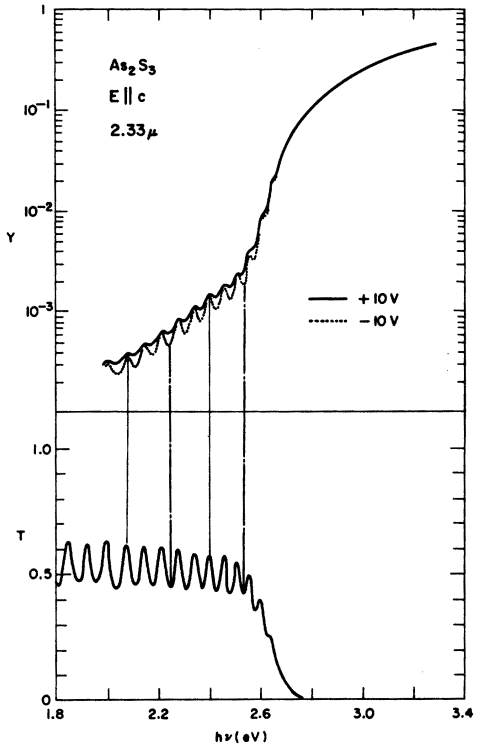

FIG. 6. Photoyield (Y) and transmission (T) spectra for $\vec{E} \parallel \vec{c}$.

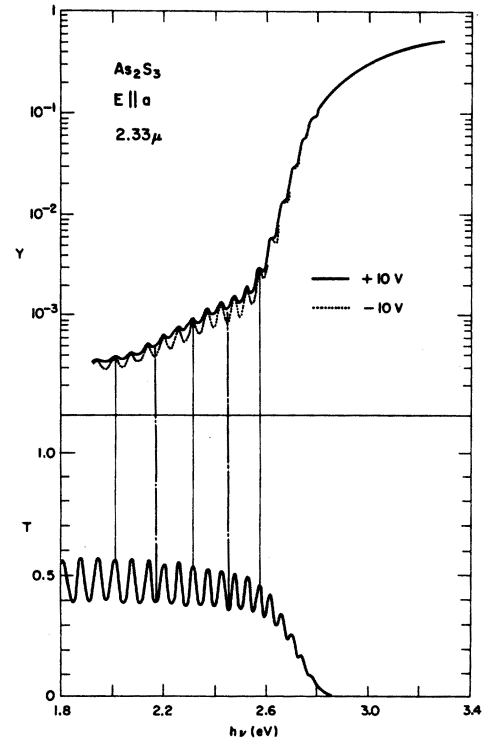

FIG. 5. Photoyield (Y) and transmission (T) spectra for $\vec{E} \parallel \vec{a}$.

by a Keithley 610BR electrometer.

Photocurrent spectra of As_2S_3 crystals were measured for both polarizations of incident light with respect to the layer plane ($\vec{E} \parallel \vec{c}$, $\vec{E} \parallel \vec{a}$), and for both field polarities relative to the illuminated surface. The samples were cleaved to thicknesses of 1–6 μm and their thicknesses calculated from the positions of the interference maxima in the transmission spectra combined with known refractive index data.[9] The refractive-index data for $\vec{E} \parallel \vec{c}$ and $\vec{E} \parallel \vec{a}$ are shown as a function of photon energy in Fig. 3. The calculated thicknesses are considered to be accurate within 5% because this was the maximum deviation between thicknesses calculated from the interference peaks in the $\vec{E} \parallel \vec{c}$ and $\vec{E} \parallel \vec{a}$ transmission spectra. Typical photoyield spectra (photocurrent normalized to the incident photon flux), obtained using 1-M NaI aqueous electrodes, are shown in Fig. 4. The photocurrents are shown for both in-plane polarizations of the incident light with the current direction being normal to the layers (along the b crystal axis). Also included in the figure are the edge-absorption spectra of crystalline As_2S_3 for the two in-plane polarizations and the absorption spectrum of amorphous As_2S_3. The dichroism of this highly anisotropic crystal is easily seen from these spectra, with the optical gaps, $h\nu$ at $\alpha = 10^4$ cm^{-1}, occurring

near 2.8 eV for $\vec{E} \parallel \vec{a}$ and 2.7 eV for $\vec{E} \parallel \vec{c}$. The photocurrents follow the edge-absorption spectra near and above the absorption edge, but not at lower photon energies. The photoyield displays a long tail, extending well below the threshold for bulk absorption, which is not polarization dependent and which has a shape somewhat similar to the amorphous absorption edge shown in Fig. 4. In Sec. III we will show that this long-wavelength photoresponse is due to electron injection from surface states.

III. SURFACE PHOTORESPONSE

Because the crystals used in this study were cleaved to thicknesses (1–6 μm) which were only a few times the optical wavelengths propagating in the solid, easily resolvable light-intensity modulations were superimposed on all spectra due to interference effects from multiple internal reflections from the crystal surfaces. These interference effects are even more pronounced because of the large refractive-index mismatch at crystal-air, crystal-liquid interfaces and also because of the optical flatness of the cleaved surfaces.

In the photocurrent spectra shown in Fig. 4, the interference oscillations in the transparent regime were intentionally suppressed so that the spectra would not depend on sample thickness. The as-measured photocurrent and transmission spectra of specific samples are shown in Figs. 5 and 6 for the two polarizations, $\vec{E} \parallel \vec{a}$ and $\vec{E} \parallel \vec{c}$, in the layer plane. Again, the photocurrent spectra

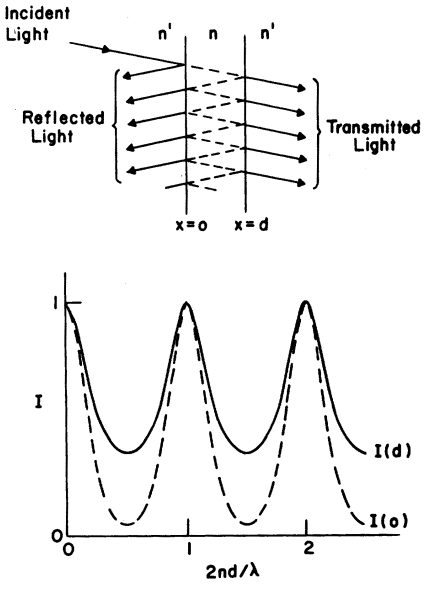

FIG. 7. Spatial dependence of interference effect showing light intensity spectra at front $I(0)$ and back $I(d)$ surfaces.

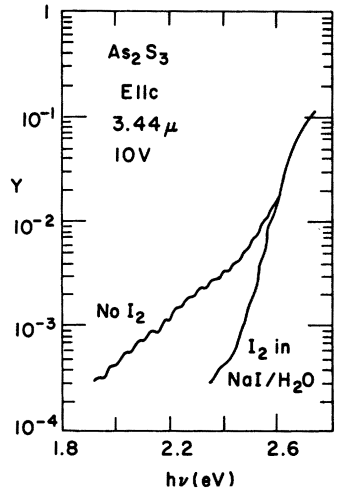

FIG. 8. Iodine quenching of electron injection from surface states in crystalline As_2S_3.

follow the edge-absorption spectra near the edge, $h\nu > 2.6$ eV, but not for lower photon energies. In the crystal's transparent region, the photocurrents exhibit interference peaks in a one-to-one correspondence to those seen in transmission. This long-wavelength photoresponse decreases only gradually with decreasing photon energy, in pronounced contrast to the optical absorption of the bulk crystal which plummets steeply to negligible values in this region. Also, as shown in Fig. 4, the long-wavelength photoresponse, after interference effects are averaged out, is polarization independent. (The different refractive indices for $\vec{E} \parallel \vec{c}$ and $\vec{E} \parallel \vec{a}$ do cause the interference oscillations to display different spacings and amplitudes for the two polarizations.) Similar photocurrent spectra have been observed in silicon[14] and amorphous germanium.[15] The very existence of a photoresponse in the absence of bulk absorption, as well as the polarization independence of this long-wavelength response, in themselves suggest an injection process; but we will see that the interference effect provides us with even more specific and unmistakeable evidence for this.

Examination of the less-than-band-gap photocurrents of Figs. 5 and 6 reveals a definite bias dependence of the amplitude of the interference oscillations in the photocurrent spectra. When a negative voltage is applied to the illuminated surface, the interference minima are deeper than those observed when the bias is reversed (or when the cell is turned around). If the currents are produced in the bulk there should be no change upon bias reversal, so that the effect must be of surface origin. But why should a surface effect exhibit a difference upon bias reversal since the liq-

uid electrode cell is symmetric and the crystalline surfaces are identical? (The crystal symmetry of As_2S_3 is centrosymmetric.) The answer lies in the fact that the optical excitation is effective in creating photocarriers at only one of the two surfaces and the interference effect on the light intensity is not the same at the two surfaces. Let us now calculate the light intensity as a function of wavelength, for wavelengths at which bulk absorption is negligible, at both the front and back surfaces. This analysis will show that the light intensity is more strongly modulated by the interference at the front surface than it is at the back surface, with deeper minima and the same maxima. In fact, the interference effect tells us that the *less-than-band-gap photocurrents always originate at the negatively biased surface*. This may be seen as follows:

Figure 7 contains a schematic representation of the multiple reflections and transmissions occurring when a nonabsorbing material of thickness d and refractive index n intercepts a light beam propagating in a medium of refractive index n'. The rays are shown at nonnormal incidence only for illustration purposes; the calculations are done assuming *normal incidence*. If the incident beam has an amplitude (electric vector) of unity and the primary reflected and transmitted beams at $x=0$ have amplitudes r and t, respectively, then the boundary conditions requiring continuity of transverse electric vector and power flow give

$$1-r=t \quad \text{and} \quad n'=n'r^2+nt^2, \quad n'\to n$$

where we have arbitrary defined the reflected beam's electric vector to be inverted with respect to the incident beam. Similarly, since the amplitude of the primary beam incident on the second surface, at $x=d$, has amplitude t, we define the amplitudes of the primary reflected and transmitted beams at $x=d$ to be tr' and tt', respectively. Then the boundary conditions requiring continuity of the transverse electric vector and power flow give equations similar to those above, or

$$1-r'=t' \quad \text{and} \quad n=nr'^2+n't'^2, \quad n\to n'.$$

All subsequent reflections must satisfy the identical boundary conditions with the relative amplitudes being $(1, r, t)$ when the wave passes from $n'\to n$ and $(1, r', t')$ when the wave passes from $n\to n'$. Solving the above equations we find that

$$r=-r'=\frac{n-n'}{n+n'}$$

and

$$nt=n't'=\frac{2nn'}{n+n'} \quad .$$

Calculating intensities at the two surfaces involves summing all the amplitudes including appropriate phase factors. Rays which have undergone multiple internal reflections will have a phase ϕ_m relative to other beams at the same surface given by

$$\phi_m=m\beta, \quad \beta=2\pi(2nd/\lambda), \quad \text{and} \quad m=\text{integer}.$$

For instance, the electric vector $E(0)$ at $x=0^-$, is given by the sum of all the electric vectors at that point in space:

$$E(0)=1-r-r'tt'e^{i\beta}-r'^3tt'e^{2i\beta}-r'^5tt'e^{3i\beta}-\cdots$$
$$=(1-r)(1+re^{i\beta})/(1-r^2e^{i\beta}) \ .$$

Similarly at $x=d+$,

$$E(d)=tt'+r'^2tt'e^{i\beta}+r'^4tt'e^{2i\beta}+\cdots$$
$$=(1-r)(1+r)/(1-r^2e^{i\beta}),$$

whereby the light intensities are given by

$$I(0)=|E(0)|^2=(1-r)^2$$
$$\times(1+r^2+2r\cos\beta)/(1+r^4-2r^2\cos\beta),$$

$$I(d)=|E(d)|^2=(1-r^2)^2/(1+r^4-2r^2\cos\beta),$$

where $\beta=4\pi nd/\lambda$, $r=(n-n')/(n+n')$, and λ is the wavelength of light. These two functions are plotted in Fig. 7 as a function of wavelength for the sample case of $n=3$ and $n'=1$. The effect on the light intensity at the two surfaces is quite dramatic and indeed we see that the predicted light intensity maxima are the same at the two surfaces but that the minima are much deeper at the front surface than at the back. For As_2S_3, the long-wavelength refractive indices are 2.97 for $\vec{E}\parallel\vec{a}$ and 2.65 for $\vec{E}\parallel\vec{c}$.[9] The refractive indices increase appreciably across the visible as in apparent from the changing frequency of oscillations in Figs. 5 and 6. The aqueous 1-M salt solution has a constant refractive index of 1.34 in the visible.

Using the above equations, we are now in a position to understand the bias dependence of the long-wavelength photoresponse of crystalline As_2S_3. We have argued that the bias dependence (plus the negligible bulk absorption) in the photoresponse tails in Figs. 5 and 6 excludes bulk effects, leaving only surface effects. Since the two surfaces are identical chemically, we have looked elsewhere and found that there is an asymmetry in the interference effect. Specifically, from the above equations it follows that the intensity maxima ($\cos\beta=1$) at the front and back surfaces are of equal amplitude but that the intensity minima ($\cos\beta=-1$) are deeper at the front surface than at the back. Since the polarity dependences of Figs. 5 and 6 show that the interference oscillations are strong when the front surface is negatively biased and weak when the back surface is negatively biased, it follows that the long-wavelength photo-

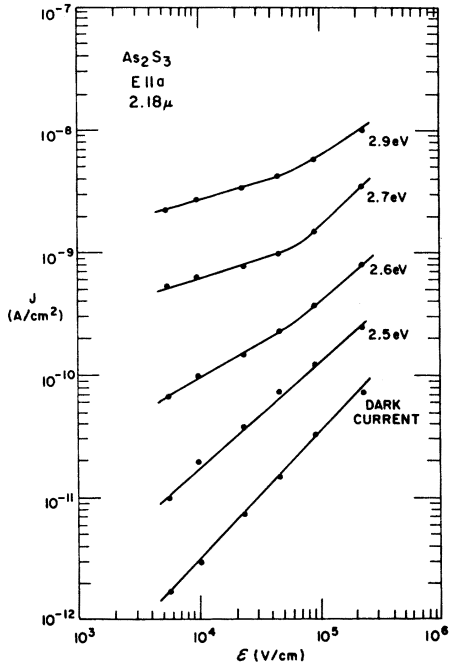

FIG. 9. Field dependence of current density in the dark and at different photon energies.

currents originate at the negatively biased surface. This means that the less-than-band-gap photoresponse corresponds to *electron photoinjection from surface states*.

A related experiment, to be described in detail elsewhere,[16] should be mentioned here because it provides striking confirmation of the above interpretation. It is known that atomic iodine can be produced by photodissociation of I_2 molecules in solution, and that such free iodine is a powerful electron scavenger. Figure 8 shows the results of a photoresponse experiment on As_2S_3 in which iodine has been introduced into the back electrolyte (i.e., liquid *B* of Fig. 2). With the back surface biased negatively so that the electron injection is from the back surface, the presence of iodine causes a dramatic quenching of the electron-injection photocurrent. This means that the iodine radicals, formed by photodissociation of I_2 in solution, effectively deplete the surface states of electrons. This is dramatic evidence for the long-wavelength photoresponse not only being a surface effect but also it being photoinjection of surface electrons (not holes).

IV. BULK PHOTORESPONSE

Measuring steady-state photocurrents is the most direct method of examining the carrier-generation step. If a carrier is generated (escapes initial recombination), and is not trapped in surface or deep bulk traps, it will transit the solid and during this process will be measured as current. The major difficulty in the interpretation of steady-state currents is the possibility of trapping which can occur either in the bulk or at the surface (contact). If a significant fraction of a CV's worth of charge is trapped the internal field will be difficult to define. This effect is usually recognized by photocurrent decay from its initial value, when the light is first turned on, to a lower steady-state value. It is important that the current be observed during the first few transits to make an unambiguous interpretation. Secondly, if trapped charge accumulates at one of the contacts, secondary injection can ensue[17] leading to photoinduced currents not directly related to the primary generation step. These currents should show the classic gain-current time response[18] starting at a low value of current and increasing to a higher steady-state value. These high-gain photocurrents will not show linear light-intensity dependencies.

The field dependence of the light and dark currents in crystalline As_2S_3, using aqueous salt solutions as transparent electrodes, is shown in Fig. 9. The sample used for these data showed very little change in photocurrent between initial and steady-state value. The transient currents showed a small amount of initial bulk trapping with the traps being filled by much less than a CV's worth of charge.[11] With the linear light-intensity dependence shown in Fig. 10, it is concluded that the steady-state photocurrent is determined solely by the generation step. Secondly, because crystalline As_2S_3 is such a good insulator with very few traps, the amount of internal charge is not sufficient to affect the internal fields so that the internal field is equal to the applied voltage divided by the sample thickness. From Fig. 9, the ap-

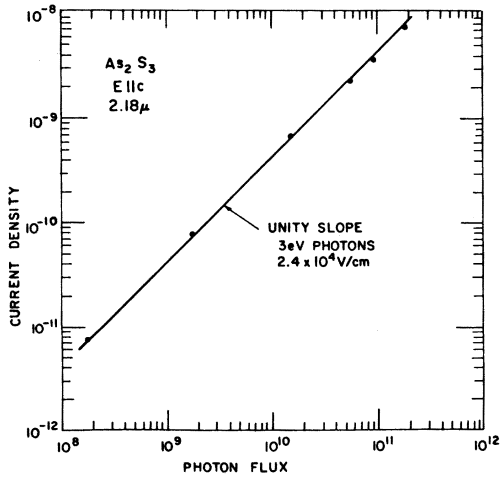

FIG. 10. Photocurrent density as function of light intensity for strongly absorbed (3 eV) photons.

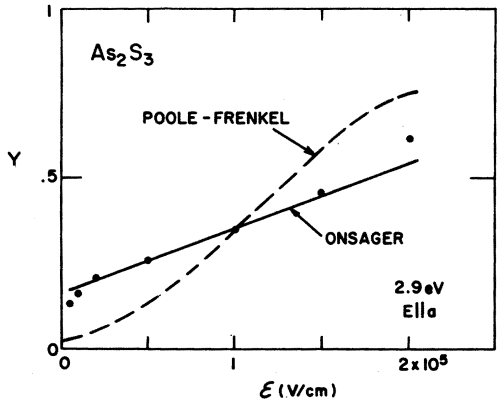

FIG. 11. Comparison of Poole-Frenkel and Onsager theoretical fits to field dependence of photoyield for strongly absorbed (2.9 eV) photons.

parent dark resistivity perpendicular to the layer planes is 3×10^{15} Ω cm. With the knowledge that the internal field is simply $E = V/d$ and that the current is generation limited, we can now examine the field dependence of the carrier generation step.

The surface photoresponse (2.5-eV curve in Fig. 9) is linear with field and is consistent with the field dependence of injection currents.[19] For strongly absorbed light (2.9-eV curve in Fig. 9), the photocurrent shows a zero-field intercept plus a linear field term consistent with the Onsager model.[6,7] This is shown in Fig. 11. The Onsager model predicts

$$Y = \exp\left(\frac{-e^2}{\epsilon r k T}\right)\left(1+\frac{e^3 E}{\epsilon (kT)^2}+\cdots\right),$$

where r is the initial thermalization length. Taking $\epsilon = 6$ for the b crystalline direction,[3] the Onsager theory fits the data for an initial thermalization length $r = 40$ Å. Considering that r is the only adjustable parameter this is an extremely good fit. Using the Poole-Frenkel model,[4] where a balance of emission and recombination rates gives

$$Y^{-1} = 1 + A\exp\left\{-\left(\frac{e^3 E}{\epsilon (kT)^2}\right)^{1/2}\right\},$$

the field dependence is simply too strong to fit the data.

The Onsager model divides the generation step into three parts: (i) creation of a hot-electron–hole pair through optical excitation, (ii) scattering by lattice vibrations or defects causing thermalization of the pair at some initial separation, and (iii) motion of carriers by diffusion and drift in the pair's mutually attractive potential plus applied potential. The ultimate fate of any carrier pair is either recombination or dissociation. As shown by Onsager[20] for a three-dimensional Coulombic potential, the recombination rate is field independent whereas the dissociation rate has a finite zero-field value and increases with the applied field. In other work, it is discussed how the thermalization length is related to the microscopic mobility.[21]

Comparing crystal and amorphous results, we find that the major effect of disorder on the transport is a large increase in the number of traps.[5] This is true also for Se which changes from a band-like drift mobility in the crystal[22] to a trap-controlled mobility in the amorphous form.[23] This is supported by the sublinear light-intensity dependence observed[5] in amorphous As_2S_3 as opposed to the linear light-intensity dependence in the crystal reported here. Reports on the carrier drift mobilities,[11] internal photoemission,[24] and ac conductivity[3] in crystalline As_2S_3 are forthcoming.

V. SUMMARY

By close examination of the photoresponse spectra of the layer crystal As_2S_3 we have been able to distinguish surface and bulk photoresponse, the surface photoresponse appearing in the spectral region in which there is no bulk photoresponse. By making use of a unique bias-dependent interference effect, the surface photoresponse has been identified as electron injection from surface states. Additional evidence for this mechanism was provided by a photoresponse quenching experiment in which electron-scavenging radicals were used to quench the surface photoresponse, with positive results. The surface photoresponse shows a linear field dependence consistent with a one-dimensional Onsager model[21] and the bulk photoresponse shows a field dependence consistent with three-dimensional Onsager theory,[6,7,20] but not consistent with Poole-Frenkel models.[4] From Onsager theory a thermalization length for hot carrier pairs is calculated to be 40 Å. The dark resistivity perpendicular to the layers is measured to be 3×10^{15} Ω cm.

[1]R. Zallen, M. L. Slade, and A. T. Ward, Phys. Rev. B 3, 4257 (1971); R. Zallen, in *Proceedings of the Enrico Fermi Summer School on Lattice Dynamics and Intermolecular Forces, Varenna*, 1972, edited by S. Califano (Academic, New York, 1973); R. Zallen and M. L. Slade, Phys. Rev. B 9, 1627 (1974).

[2]A. I. Lakatos and M. Abkowitz, Phys. Rev. B 3, 1791 (1971).

[3]M. Abkowitz, D. F. Blossey, and A. I. Lakatos (unpublished).

[4]R. C. Enck, Phys. Rev. Lett. 31, 220 (1973); D. M. Pai and S. W. Ing, Jr., Phys. Rev. 173, 729 (1968); M. D. Tabak and P. J. Warter, *ibid.* 173, 899 (1968).

[5]S. W. Ing, Jr., J. H. Neyhart, and F. W. Schmidlin,

J. Appl. Phys. 42, 696 (1971).
[6]P. J. Melz, J. Chem. Phys. 57, (1972).
[7]R. H. Batt, C. L. Braun, and J. F. Hornig, J. Chem. Phys. 49, 1967 (1968); Appl. Opt. Suppl. 3, 20 (1969); R. R. Chance and C. L. Braun, J. Chem. Phys. 59, 2269 (1973).
[8]N. Morimoto, Mineral J. 1, 160 (1954).
[9]B. L. Evans and P. A. Young, Proc. R, Soc. A 297, 230 (1967).
[10]R. Zallen, R. E. Drews, R. L. Emerald, and M. L. Slade, Phys. Rev. Lett. 26, 1564 (1971); R. E. Drews, R. L. Emerald, M. L. Slade, and R. Zallen, Solid State Commun. 10, 293 (1972).
[11]D. F. Blossey and R. C. Enck (unpublished).
[12]R. G. Kepler, Phys. Rev. 119, 1226 (1960).
[13]R. Raman and S. P. McGlynn, Spectroscopy Lett. 3, 221 (1970).
[14]W. Muller and W. Monch [Phys. Rev. Lett. 27, 250 (1971)] interpret the oscillations in their photocurrent spectra of freshly cleaved silicon in terms of phonon-assisted transitions, invoking as many as *nine* optical phonons with all peaks equal in size. However a 3-μm surface layer, possibly a depletion region, with a different refractive index than the bulk would cause interference oscillations of precisely this sort. Interference effects due to surface regions are reported by F. Evangelisti, A. Frova, and J. U. Fishbach [Phys. Rev. Lett. 29, 1001 (1972)].
[15]J. E. Fischer, Phys. Rev. Lett. 27, 1131 (1971).
[16]D. F. Blossey, Chem. Phys. Lett. 25, 593 (1974).
[17]R. R. Mehta and B. S. Sharma, J. Appl. Phys. 44, 325 (1973).
[18]R. H. Bube, *Photoconductivity of Solids* (Wiley, New York, 1960), p. 287.
[19]J. Mort, F. W. Schmidlin, and A. I. Lakatos, J. Appl. Phys. 42, 5761 (1971).
[20]L. Onsager, Phys. Rev. 54, 554 (1938); J. Chem. Phys. 2, 599 (1934).
[21]D. F. Blossey, Phys. Rev. B (to be published).
[22]J. Mort, J. Appl. Phys. 39, 3543 (1967); Phys. Rev. Lett. 18, 540 (1967).
[23]M. D. Tabak, Phys. Rev. B 2, 2104 (1970).
[24]D. F. Blossey (unpublished).